Analysis of Metal Transfer in Gas Metal Arc Welding

This study shows that the transition of metal transfer mode in gas metal arc welding occurs much more gradually than is generally believed

BY Y-S. KIM AND T. W. EAGAR

ABSTRACT. Droplet sizes produced in GMAW are predicted using both the static force balance theory and the pinch instability theory as a function of welding current, and the results are compared with experimental measurements. The causes for the deviation of predicted droplet size from measured size are discussed with suggestions for modification of the theories in order to more accurately model metal transfer in GMAW. The mechanism of repelled metal transfer is also discussed. The transition of metal transfer mode has been considered as a critical phenomenon which changes dramatically over a narrow range of welding current. This transition has been investigated experimentally using high-speed videography which shows that the transition is much more gradual than is generally believed. The mechanism of the transition is discussed using a modified static force balance theory.

Introduction

In gas metal arc welding (GMAW), there are various modes of metal transfer such as globular, repelled globular, projected spray, streaming, and rotating transfer. These transfer modes show different arc stabilities, weld pool penetrations, spatter production, porosity population and level of gas entrapment. Lesnewich (Ref. 1) showed that the mode of metal transfer depends on many operational variables such as welding current, electrode extension, electrode diameter and polarity. Later, A. A. Smith (Ref. 2) reported that an entirely different type of metal transfer mode is produced when using carbon dioxide gas shielding as compared with argon shielding.

With many factors influencing metal transfer, theoretical models such as the static force balance theory (Refs. 3–5) and the pinch instability theory (Refs. 6–8) have been proposed to explain the metal transfer phenomenon. These have had limited success.

Y. S. KIM is Assistant Professor, Department of Metallurgy and Materials Science, Hong Ik University, Seoul, Korea. T. W. EAGAR is Co-Director, Leaders for Manufacturing Program, Richard P. Simmons Professor of Metallurgy, Department of Materials Science and Engineering, Massachusetts Institute of Technology, Cambridge, Mass.

KEY WORDS

Modeling
GMAW Metal Transfer
Droplet Size Predict
Transfer Frequency
Taper Formation
Shielding Gas
Electrode Extension
Static Force Bal. Theory
Pinch Instability Theory
Measurement

In this study, the droplet size and droplet transfer frequency are analyzed both theoretically and experimentally. In the first section of this paper, the equilibrium drop sizes are calculated using the static force balance analysis and the pinch instability analysis. In the second section of this paper, measurements of droplet size at different welding currents are compared with the theoretical predictions. The limitations of the static force balance theory and the pinch instability theory in the prediction of the droplet size are discussed. In order to account for the deviation between these theories and the experimental data, a modification of the static force balance theory is proposed. The modified theory is tested using a pulsed current welding experiment.

Previous Studies

Factors Affecting Metal Transfer Modes

The operational variables affecting the mode of metal transfer are the welding current, composition of shielding gas, extension of the electrode beyond the current contact tube, ambient pressure, active element coatings on the electrode, polarity, and welding material. Among these variables, welding current is the most common variable that the welder adjusts to obtain the desired metal transfer mode. At low welding currents, globular transfer mode occurs, while spray transfer mode occurs at relatively higher welding currents.

At the lower welding current range of the spray transfer mode, projected transfer occurs in which the droplet diameter is approximately the same as the diameter of the electrode. As the welding current increases, the metal transfer mode changes from projected transfer mode to streaming transfer mode, then to a rotational transfer mode. This sets a practical upper limit on the current because unstable metal transfer begins with rotational transfer.

The transition of metal transfer modes described above are observed in sequence only when the welding material is steel and the shielding gas has an argon-rich composition. With other materials and with other shielding gases, not all metal transfer modes are observed. When carbon dioxide, helium, and nitrogen are used as shielding gases, the repelled globular transfer mode is usually observed (Refs. 9–11) and neither streaming transfer nor rotational transfer is observed. When mixtures of argon and carbon dioxide are used, the rate of drop transfer was found to increase linearly with the composition of the argon gas (Ref. 12).

Considering the effects of shielding gas on the metal transfer modes described above, there have been several attempts to increase the workable range of welding current by suppressing the rotational transfer mode using argon-based shielding (Ref. 13). When helium and/or carbon dioxide are added to the argon gas, the range of welding current for projected spray transfer is greatly increased.

In addition, when a shorter electrode extension and a larger electrode diameter are used, the transition current is increased (Ref. 1). Amson (Ref. 14) observed that as the pressure increases, the transition current increases. However, Perlman, *et al.* (Ref. 15), found that when the pressure reaches 5 atm, spray transfer becomes irregular and fluctuation of the voltage increases. The use of thin coatings on the electrode consisting of alkali, alkaline earth, rare earth elements, and certain oxides have been shown to increase the stability of metal transfer (Refs. 16-18).

Review of Existing Theories of Metal Transfer

There are two well-quoted theories of metal transfer. These are the static force balance theory (Refs. 3–5) and the pinch instability theory (Refs. 6–8). In addition to these theories, the plasma force theory (Ref. 19) and the critical velocity theory (Ref. 20) have been proposed to explain the transition between metal transfer modes.

1) Static Force Balance Theory. The static force balance theory postulates that the drop detaches from the electrode when the static detaching forces on the drop exceed the static retaining force. Four different forces are usually considered: the gravitational force, electromagnetic force, and plasma drag force are detaching forces, while the surface tension force is a retaining force. The gravitational force is due to the mass of the drop and acts as a detaching force when welding in the flat position:

$$F_g = \frac{4}{3}\pi R^3 \rho_d g \qquad (1)$$

where R is the droplet radius, ρ_d is the density of the drop, and g is the gravitational constant.

The electromagnetic force on the drop results from divergence or convergence of current flow within the electrode. When the current lines diverge in the drop, the Lorentz force, which acts at right angles to these current lines, creates a detaching force. The electromagnetic force is given by Lorentz's law:

$$F_m = \bar{J} \times \bar{B} \qquad (2)$$

where $\bar{J}$ is current density and $\bar{B}$ is magnetic flux.

By assuming that the current density on the drop is uniform, the total electromagnetic force on a drop can be obtained by integrating Equation 2 over the current conducting surface of the drop (Ref. 3).

$$F_{em} = \frac{\mu_0 I^2}{4\pi} f_2$$

$$\text{where } f_2 = \left[\begin{array}{l} ln\dfrac{R\sin\theta}{r} - \dfrac{1}{4} - \dfrac{1}{1-\cos\theta} \\ + \dfrac{2}{(1-\cos\theta)^2} ln\dfrac{2}{1+\cos\theta} \end{array} \right] \qquad (3)$$

where I is the welding current and μ_0 is the permeability of free space. The geometry used in Equation 3 and a graph of f_2 as a function of the conduction zone angle is given in Fig. 1. When the conduction zone is small such that the current lines converge, f_2 becomes negative, *i.e.*, the electromagnetic force acts as a repulsive force. However, when the conduction zone is large enough so that the current lines diverge, f_2 becomes positive and the electromagnetic force becomes a detaching force.

The plasma drag force on the liquid drop can be estimated by considering the drag force on a sphere immersed in a fluid. The drag force on a sphere immersed in a fluid of uniform velocity field is (Ref. 23)

$$F_d = C_D A_p \left(\frac{\rho_f v_f^2}{2} \right) \qquad (4)$$

where C_D is the drag coefficient, A_p is the projected area on the plane perpendicular to the fluid flow, ρ_f is the density of the fluid, and v_f is the velocity of the gas. Therefore, the plasma drag force acting on the liquid drop can be approximated by modifying Equation 4 to allow for the area occupied by the electrode.

The surface tension force, which acts to retain the liquid drop on the electrode is given as follows:

$$F_s = 2\pi\alpha\gamma \qquad (5)$$

where α is the radius of the electrode and γ is the surface tension of the liquid metal.

Waszink (Ref. 22) investigated the relative magnitudes of the detaching forces and showed good agreement with experimental results within the range of globular transfer, however, in the spray transfer mode, the theory deviates significantly from the experiment.

In addition to the above-mentioned limitations, the static force balance theory has difficulties in explaining several metal transfer phenomena in GMAW. Firstly, the effect of electrode extension on metal transfer is difficult to explain since the electrode extension will not affect the force balance. Secondly, the analyses of metal transfer using this theory have been performed mostly using steel electrodes and argon shielding gas. Other systems which produce a repelling transfer mode cannot be explained with this theory.

2) Pinch Instability Theory. The pinch instability theory was developed from the Rayleigh instability model (Ref. 23) of a liquid cylindrical column. Since spheres can have a lower free energy than the liquid column, a disturbance of the proper wavelength in the liquid column tends to cause the liquid column to break up into drops. Rayleigh derived the conditions for the liquid column instability assuming a simple sinusoidal perturbation for an invicid system. The perturbation of the cylinder is solved with an exponential function of the form

$$\alpha_m(t) = e^{i\omega t} \qquad (6)$$

$$\text{where } \omega^2 = \frac{\gamma\eta}{\rho\alpha^3}\left(1 - m^2 - \eta^2\right)\frac{I_m'(\eta)}{I_m(\eta)}$$

$$\eta = \frac{2\pi\alpha}{\lambda} \qquad (7)$$

ρ = density, λ = wavelength of the fluctuation, $I_m(\eta)$ = modified Bessel function of the first kind order m, $I'_m(\eta)$ = the first derivative of $I_m(\eta)$.

When m = 0 (sausage mode), the maximum frequency is obtained with η = 0.696, and the most probable drop size (R_o) is calculated to be twice the diameter of the liquid column.

The pinch instability theory of metal

transfer analysis postulates that the pinch force on the liquid column of molten metal due to the self-induced electromagnetic force enhances the break-up of the liquid column into droplets. An approximate analytical solution of the critical wavelength of this instability has been derived (Ref. 24) :

$$\lambda_c = \frac{2\pi\alpha}{\left(1 + \frac{\mu_0 I^2}{2\pi^2 R_\gamma}\right)^{1/2}} \qquad (8)$$

As seen in Equation 8, the welding current reduces the critical wavelength of the instability of the liquid jet and thus decreases the droplet size. In this way, the pinch instability theory claims to explain the general trend of decreasing drop size with increasing welding current.

Anno (Ref. 25) derived the frequency of fluctuation for a viscous jet with a surface charge and showed that viscous effects and surface charges have stabilizing effects. Allum (Ref. 8) showed that the viscous effects are negligible in liquid metal, but the stabilizing effects of surface charge are significant in the low welding current range.

The pinch instability theory suffers the same problems as the static force balance theory. These include difficulties in explaining the effect of electrode extension, and the repelling mode of metal transfer.

3) Other Theories. When using steel electrodes with argon shielding, the transition of metal transfer mode from globular to spray transfer has been reported to occur over a very narrow current range: less than 10 A (Ref. 1). In an attempt to explain the sharp transition in metal transfer mode as found by Lesnewich (Ref. 1), Needham, *et al.* (Ref. 19), using the static force balance theory, has proposed that the transition occurs when the welding plasma starts to exert a drag force on the drop.

Calculation of Equilibrium Drop Size

From the static force balance theory, the droplet size can be calculated under the assumption that the drop detaches from the electrode when the sum of the detaching forces equals the holding force :

$$\underset{\text{(holding force)}}{F_\gamma} = \underset{\text{(detaching force)}}{F_{em} + F_g + F_d} \qquad (9)$$

In calculating these forces acting on the liquid drops, a number of assumptions are made. Firstly, in calculating the electromagnetic force on the droplet, the electrons are assumed to condense uniformly on the liquid droplet only and

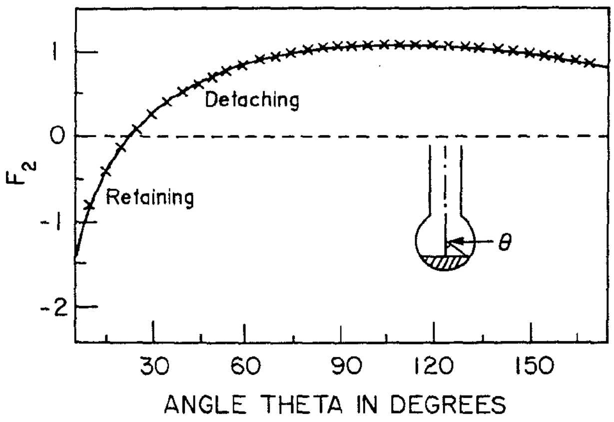

Fig. 1 — Variation of f_2 as a function of q value.

θ is assumed to be 150 deg, which is the conduction zone angle when the droplet size is twice the size of the electrode. As seen in Fig. 1, the value of f_2 does not change significantly when θ is larger than 60 deg. Thus, this assumption will not cause any significant error in the electromagnetic force calculation.

For the drag force, the value of C_D in Equation 4 depends on the Reynold's number of the shielding gas. Since the velocity of the plasma in GMAW is not available, the plasma velocity was assumed to be 100 m/s, which is the same as the plasma velocity in GTAW (Ref. 27). The Reynold's number with this velocity is calculated to be approximately 9000, which lies in the Newton's law region. Thus, the values of C_D for the plasma is 0.44 (Ref. 21). For less-developed plasma jets, 10 m/s was used for the velocity of the fluid. The value C_D for 10 m/s gas flow rate is also calculated to be 0.44. A_p is the projected area of the sphere exposed to the fluid on a plane perpendicular to the direction of the motion and is given by Equation 10

$$A_p = \pi\left(R^2 - \alpha^2\right) \qquad (10)$$

For the surface tension force, it is assumed that the interface between the liquid drop and solid electrode is perpendicular to the electrode axis. Also, the diameter of the drop holding neck was assumed to be the same size as the electrode diameter. The surface tension data were assumed to be: 0.9 N/m for aluminum (Ref. 27), 1.3 N/m for titanium (Ref. 28), and 1.8 N/m for steel (Ref. 27).

The total detaching force under various droplet size at a certain welding current is the summation of the electromagnetic force, the gravitational force, and the plasma drag force. At the crossover point, where the surface tension holding force and the total detaching forces meet, the equilibrium droplet size is determined. Figure 2 shows the total detaching force at various welding currents as a function of droplet size for steel electrodes with shielding gas velocities of 10 m/s, respectively. The crossover point at each welding current defines the equilibrium droplet size from the static force balance theory. The equilibrium droplet size of the steel electrode with shielding gas velocity of 10 m/s and 100 m/s are summarized in Fig. 3.

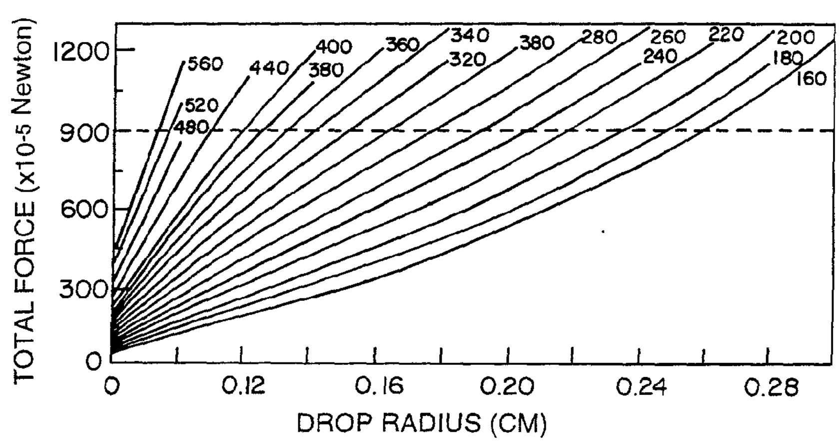

Fig. 2 — Variations of the detaching force as the droplet size at the steel electrode tip increases. The assumed argon plasma velocity is 10 m/s.

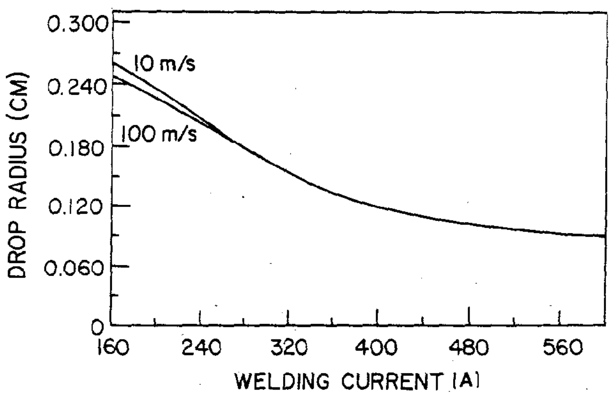

Fig. 3 — The equilibrium droplet size of the steel electrode calculated from the static balance theory. The shielding gas is assumed to be argon.

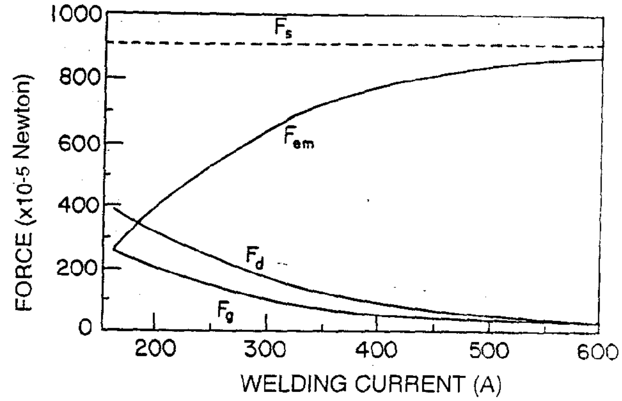

Fig. 4 — The forces acting on the drop at a steel electrode tip (argon plasma velocity: 100m/s).

The effect of velocity differences in the shielding gas is not significant and decreases as the current increases. This is because the influence of the electromagnetic force becomes dominant as current increases (Fig. 4). At low welding currents, the welding plasma does not form a strong enough jet to produce a 100 m/s velocity jet, thus, it is likely that the droplet size will follow the prediction of the 10 m/s jet. However, as the welding current increases, the droplet size will follow the prediction of the 100 m/s jet. In addition, this prediction shows that the droplet size decreases smoothly as the welding current increases.

The droplet size from the pinch instability theory is calculated using Equation 8. Assuming that the most probable wavelength of the instability is $\lambda_c/0.696$, the droplet size is calculated and plotted as a function of welding current in Fig. 5. The droplet size decreases continuously as welding current increases; however, the pinch instability theory predicts drop sizes which are much smaller than the equilibrium drop size predicted by the static force balance theory.

Experimental Procedures

Mild steel (AWS ER70S-3), aluminium alloy (AA1100, AA5356), and titanium alloy (Ti-6Al-4V) were used in the experimental portion of this study. The shielding gases used were pure argon, pure helium, 25%Ar-75%He, 50%Ar-50%He, 75%Ar-25%He, Ar-2%O_2 and carbon dioxide. The welding equipment included a constant current power supply, and a voltage controlled electrode feed with a "low inertia" motor. The transistorized welding current regulator used in this study was of the constant current type that can supply DC current with less than 1% ripple (Ref. 29). This system is capable of pulsing the DC current to a maximum of 5 kHz for small superimposed signals. The welding was performed under direct current electrode positive (DCEP) conditions. An alumina tube was inserted into the contact tube, leaving only 5 mm (0.2 in.) for contact length rather than the normal contact length of 24 mm (0.94 in.) in commercially available contact tubes. This reduced the variability in joule heating due to changes in the location of the current contact.

Analysis of metal transfer was performed using high-speed videography with a laser back-lighted shadowgraphic method (Ref. 30). In this method, a spatial filter is located at the focal point of the objective lens, where the parallel laser light becomes focused. Thus, the spatial filter transmits most of the laser light and excludes most of the intense arc light. The high-speed video camera is capable of producing images at a maximum 1000 full frame pictures per second (pps). In most of the analyses of metal transfer, this maximum 1000 pps filming rate was used. The droplet transfer rate was measured for ten seconds and an average droplet transfer rate for

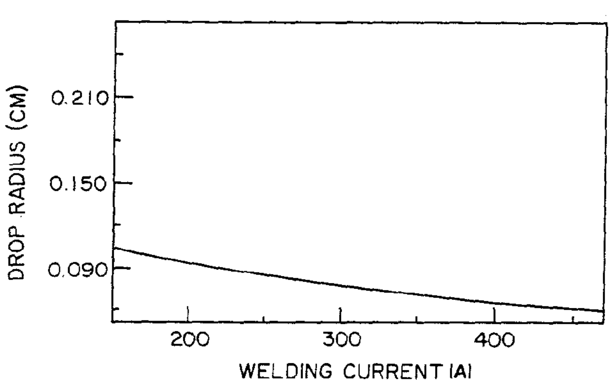

Fig. 5 — The droplet size of steel electrodes when shielded with Ar-2%O_2 calculated from the pinch instability theory.

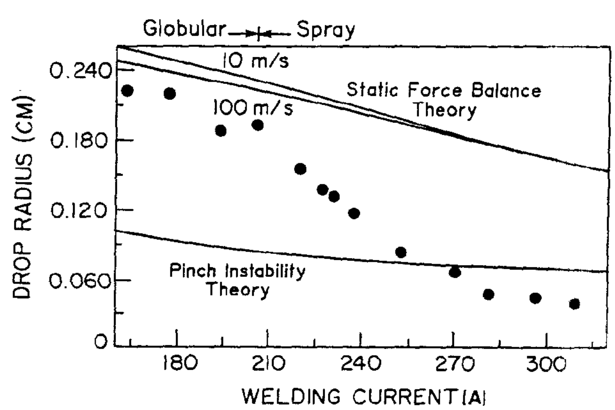

Fig. 6 — Comparison of predicted and measured droplet size of the steel electrode when shielded with Ar-2%O_2.

each welding condition was calculated. The droplet size was measured from the still image on the screen once every second for ten seconds and averaged. The variation in measured droplet size and frequency was ±5%.

The parameters used as variables in this study include welding current, welding material, shielding gas, electrode extension, and arc length. The combinations used are shown in Table 1. All the welding was performed as bead-on-plate, and the plates were prepared such that there was no mill scale on the surface. The electrode diameter used was 1.6 mm (1/16 in.) for all materials.

The arc length using argon shielding gas was constant at 14 mm (0.55 in.), but with helium and carbon dioxide shielding gas, the arc lengths were 6 and 8 mm (0.24 and 0.31 in.),respectively, because of the higher electrical resistivities of these welding plasmas.

Table 1 — The Combination of Welding Parameters Used in This Study

	Shielding Gas			Electrode Extension	Arc Length	Welding
	Argon	Helium	CO_2	(mm)	(mm)	Current
Mild steel	(a)	(a)	(a)	16,26,36	14:Ar 6:He 8:CO_2	180–420 A
Aluminum (1100,5356)	(a)			16,26,36	14:Ar	80–220 A
Ti-6Al-4V	(a)		(a)	16,26,36	14:Ar, 8 CO_2	120–260 A

(a) Welding was performed.

Measurement of Droplet Size and Transfer Frequency

Effect of Welding Current

Figure 6 shows the experimental results of droplet size measured as a function of welding current when shielded with Ar-2% oxygen gas using a 2.6 cm (1.02 in.) electrode extension. The droplet size predicted from the static force balance theory and the pinch instability theory is also shown in the figure. As seen in Fig. 6, the measured droplet size decreases gradually as welding current increases, and there is no sharp transition. In the globular transfer mode, the predicted drop size from the static force balance is reasonably close to the measured values. As the welding current increases, the predicted droplet size starts to deviate from the measured values significantly. The drop size predicted from the pinch instability theory is much too small in the globular transfer mode region and does not tend toward the experimentally determined droplet sizes at high currents.

Figure 7 shows the measured frequency of drop transfer. Again, no sign of a sharp transition in the metal transfer rate is present. Using a definition of spray transfer mode in which the droplet diameter is the same as the diameter of the electrode, one obtains a transition at a current of approximately 255 A. The transition from projected spray transfer mode to streaming transfer mode is also a gradual phenomenon. The droplet size decreases gradually, and it is very difficult to define the transition current based on either droplet size or frequency.

Effect of Shielding Gas

Figure 8 shows the repelled transfer mode just before detachment, when shielded with carbon dioxide gas. The drops are blown away from the base metal by the strong cathode jet, and they are distorted significantly. As the welding current increases, the droplet size and the distortion of the drops become less pronounced.

The average droplet size is plotted in Fig. 9 as a function of welding current with helium and carbon dioxide shielding. Because of errors in direct measurements of droplet size due to distortion, the average droplet sizes that are plotted are not the directly measured data. The average sizes were calculated by dividing the melting rate of the electrode by the frequency of metal transfer, both of which were experimentally measured. Figure 10 shows the variation of droplet transfer frequency as a function of welding current for both of the shielding gases.

With helium shielding, at low welding currents, the droplet sizes are much bigger than predicted by the static force balance theory. As the welding current increases, a change occurs in the droplet size around 240 A. This jump corresponds to the transition from the repelled globular transfer mode to the projected spray transfer mode. In the spray transfer mode, the droplet size predicted from the static force balance theory agrees fairly well with the experimentally measured droplet size. With carbon dioxide shielding, a repelled transfer mode was observed up to the maximum welding current tested in this study, *i.e.*, 400 A. The droplet size continued to decrease as the welding current increased, and there was no dramatic change in the droplet size as current was increased.

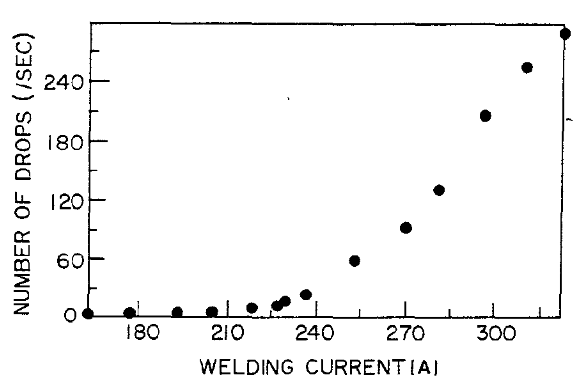

Fig. 7 — Frequency of drop transfer of the steel electrode with Ar-2%O_2 shielding.

Fig. 8 — Repelled metal transfer of steel electrodes shielded with CO_2 gas.

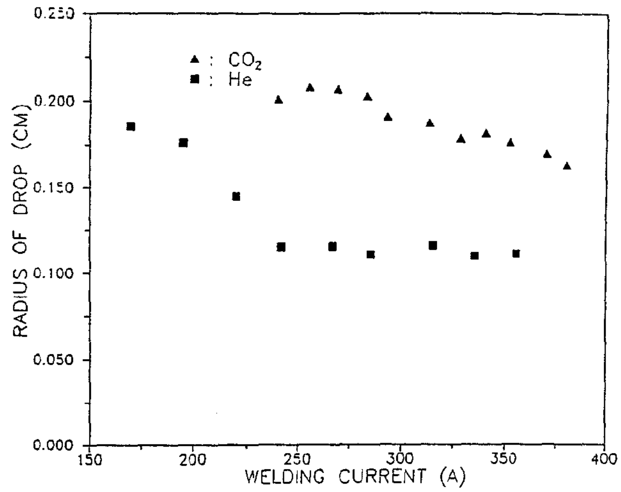

Fig. 9 — Experimentally measured droplet size for steel electrodes shielded with helium and carbon dioxide.

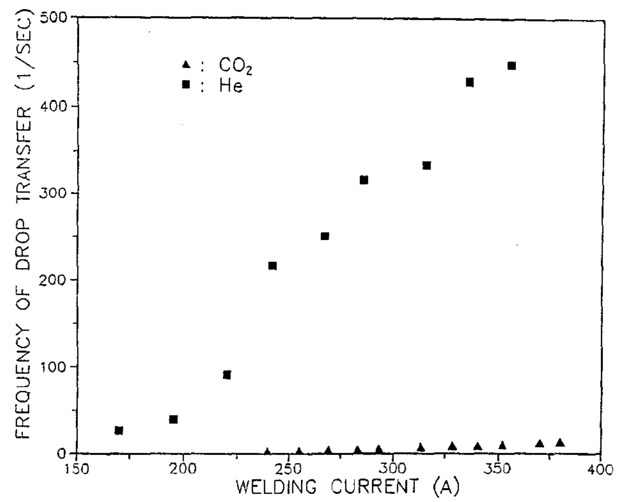

Fig. 10 — Frequency of drop transfer of steel electrodes shielded with helium and carbon dioxide.

With these shielding gases, streaming transfer mode was not observed.

In order to explain the repelled transfer mode observed with these shielding gases, it is necessary to introduce a repelling force into the static force balance theory. A possible candidate for the repelling force in helium and carbon dioxide shielding gases is the cathode jet force. The cathode jet force in GTAW has been estimated as in Equation 11 (Ref. 31).

$$F_{cathode\ jet} = \frac{\mu_0 I^2}{8\pi} \qquad (11)$$

In the range of welding current from 200 ~ 400 A, the cathode jet force is calculated to vary from 1 X 10^{-2} to 6 X 10^{-2} N, which is comparable to the detaching force.

Effect of Electrode Extension

Figure 11 shows the droplet size variation with welding current at two electrode extensions: 2.6 and 3.6 cm (1.02 and 1.43 in.). A steel electrode shielded with Ar-2% O_2 gas was used. As the electrode extension increases from 2.6 to 3.6 cm, the current of the globular-projected spray transition deceases from 255 to 240 A. As seen in Fig. 11, the effect of electrode extension on metal transfer is significant. However, this effect is very difficult to understand in terms of either the static force balance theory or the pinch instability theory. The possible cause for the effect will be discussed in a later section of this paper.

Effect of Welding Material

Metal transfer with aluminum and with Ti-6Al-4V electrodes in addition to the steel electrodes was studied. Figure 12 shows the variation of the droplet size with welding current for an aluminum electrode, along with the droplet size predicted by the static force balance theory. The transition from globular transfer to spray transfer occurs over a very narrow range of welding current in both alloys 1100 and 5356.

The droplet size in the globular range is within the range of the prediction from the static force balance theory. As the welding current increases, the droplet size from the static force balance theory deviates significantly from the experimental results as in the case of steel electrodes. The current of the globular-projected spray transfer transition was 120 A.

For the Ti-6Al-4V electrode, the measured droplet sizes are shown in Fig. 13. With this electrode, two different metal transfer modes are shown: repelled transfer due to a strong cathode jet (Fig. 14) was observed at low welding currents, and projected transfer was observed at high welding currents. As the welding current increases, there is a sudden reduction in the droplet size. This jump corresponds to the transition from the repelled globular transfer mode to the projected spray transfer mode, as is also found in steel electrodes shielded with helium gas.

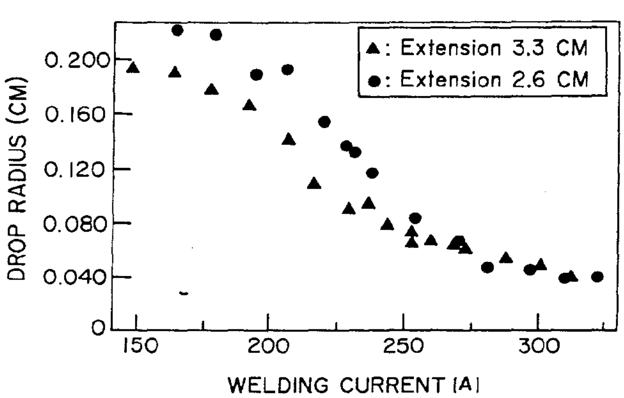

Fig. 11 — Effects of electrode extensions on the droplet size of steel electrodes. The shield gas is Ar-2%O_2.

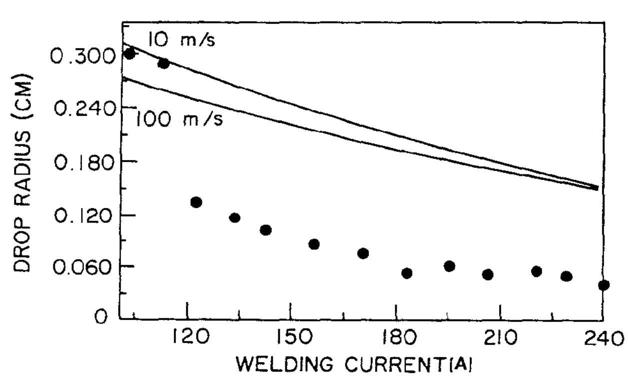

Fig. 12 — Comparison of predicted and measured droplet size of an aluminum 1100 electrode with Ar-2%O_2 shielding.

In the projected spray transfer region, the droplet size predicted by the static force balance theory predicts larger droplet sizes compared with the experimental results. It is believed that the deviation is caused by the value of the surface tension used: the surface tension for the Ti-6Al-4V alloy was unavailable and the surface tension for pure titanium was used in the calculation.

As an illustration of the strength of the cathode jet force with Ti-6Al-4V electrodes, Fig. 15 shows successive pictures of a trajectory of the drop detached from the electrode and repelled by the cathode jet in the welding plasma. The welding material used was zirconium, which has similar thermophysical properties as the Ti-6Al-4V electrode, and the shielding gas was argon.

Initially, the drop travels toward the weld pool. As it approaches the weld pool, the cathode jet becomes stronger such that the velocity of the drop is reduced and finally the drop is rejected away from the weld pool by the cathode jet, causing spatter on the base plate. This phenomenon is also frequently observed with the Ti-6Al-4V electrode. As the welding current increases, the anode jet dominates the plasma flow, and the droplet transfer mode changes from repelled transfer to projected spray transfer.

The Cause of Droplet Size Deviation between the Static Force Balance Theory and the Experimental Results

The discrepancy of the droplet size from the static force balance theory as compared with the experimental data may be explained by examining the validity of the assumptions made in the calculation of the static force balance theory. One of the most important assumptions is that the electrode should remain cylindrical and maintain its full diameter at the point where the drop is formed. If the diameter of the neck is changed either by surface melting or by deformation, the holding force will be affected as can be seen from Equation 5.

The geometry of the drop holding neck was investigated under various conditions, and it was found to be significantly changed due to formation of a taper at the electrode tip — Table 2.

As seen in Table 2, the tapering of the electrode occurs in the range of welding currents where the discrepancy between the theoretical droplet size and experimental data becomes significant. Figure 16 shows a fully developed taper at high welding current (>280 A). The tapering of the electrode occurs because the anode spot reaches this surface of the electrode and generates condensation heating on the cylindrical surface

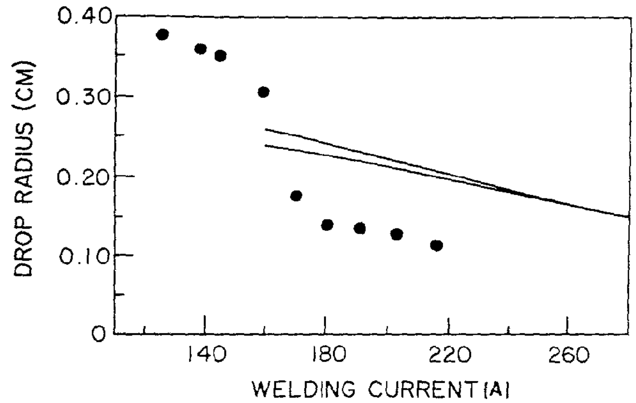

Fig. 13 — Comparison of predicted and measured droplet size of a Ti-6Al-4V electrode with Ar-2%O_2 shielding.

Fig. 14 — Repelled metal transfer of Ti-6Al-4V electrodes caused by the strong cathode jet force. The shielding gas is Ar-2%O_2 shielding.

Table 2 — Tapering of Electrode at Various Welding Currents with a Steel Electrode Shielded with Ar-2% O_2

Welding current (A)	205	237	253	281	310
Taper length (mm)	0	2.4	2.7	4.1	5.1

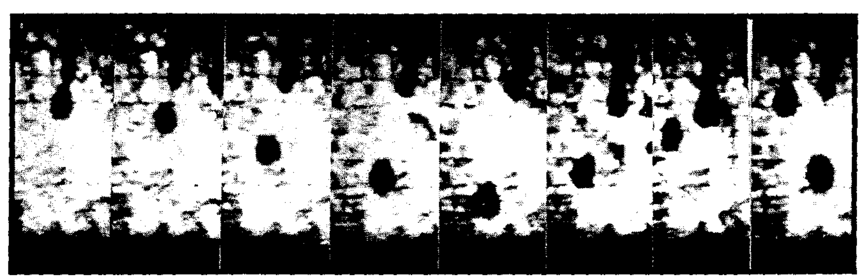

Fig. 15 — Successive pictures of a drop rejected by the strong cathode jet from the base metal. The electrode material is zirconium and the shielding gas is pure argon.

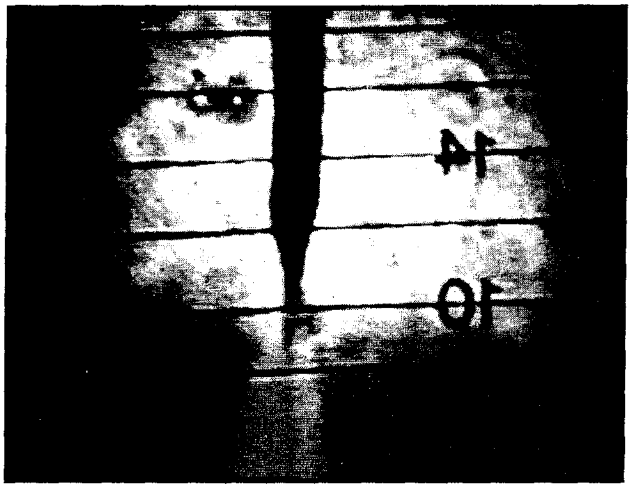

Fig. 16 — A typical shape of the taper formed at the end of steel electrode when shielded with Ar-2%O_2.

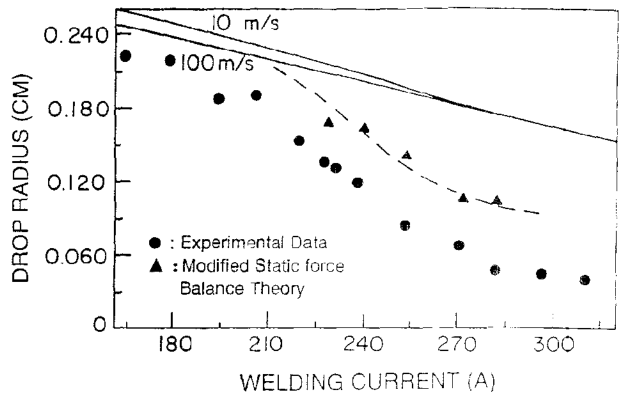

Fig. 17 — Comparison of droplet size predicted by the static force balance theory and by the modified static force balance theory with measured values.

of the electrode (Ref. 32). When enough heat is generated on the surface, the surface will melt and the liquid metal will be swept downward by either the gravitational force and/or the plasma drag force. When this melting and sweeping action occurs over a significant length of cylinder, a taper will develop at the end of the electrode.

The tapering of the electrode tip will reduce the effective diameter of the drop holding neck, thus reducing the holding force in Equation 5. The reduced holding force will produce a smaller droplet size thus creating a streaming droplet transfer mode. On the other hand, with steel electrodes shielded with helium and with Ti-6Al-4V electrodes shielded with Ar gas, tapering of the electrode is not observed, and the droplet size decrease in the spray transfer region is gradual as the static force balance theory predicts.

Considering the taper formation, the droplet size predicted from the modified static force balance theory is shown in Fig. 17. The modification was made by measuring the size of the drop holding neck at different welding currents and substituting the tapered electrode radius for the radius of the drop holding neck in Equation 5. It was assumed that most of the welding current flows directly into the drop. As seen in the figure, the droplet size predicted from the modified theory follows the measured droplet size.

The effect of the electrode extension may also be explained by considering the taper formation. The total heat input into the electrode occurs via electron condensation heat and joule heat as defined by Equation 12

$$Q_{total} = \left(\frac{3}{2}kT/e + V_a + \phi\right)I + \bar{\rho}\frac{L}{A}I^2 \quad (12)$$

where k is Boltzman's constant, T is the electron temperature entering the electrode, e is the electron charge, V_α is the anode drop voltage, ϕ is the work function of the electrode, $\bar{\rho}$ is the average resistivity of the electrode, L is the electrode extension, and A is the cross-sectional area of the electrode. The condensation heat is generated when electrons enter the electrode from the plasma. When shielded with argon, some portion of this heat enters onto the cylindrical surface since electrons condense not only on the surface of the liquid drop, but also on the surface of the solid electrode. The joule heat is the heat generated by the electrical resistance of the electrode and occurs uniformly inside the electrode.

When there is no condensation heat input on the cylindrical surface of the electrode, the temperature of the solid electrode will increase as the joule heat generation increases. Thus, with longer electrode extension, the melting of the cylindrical surface (tapering) can occur at lower surface condensation currents. This explains the results of lower transition currents for the globular-spray transfer transition with longer electrode extensions as seen in Fig. 11.

Drop Size Measured during Pulsed Current Welding

In order to test the tapering theory, pulsed current welding experiments with which tapering can be controlled were designed. The experimental procedures for the pulsed current welding may be found elsewhere (Ref. 33). Figure 18 shows the minimum droplet sizes measured at 300-, 400- and 500-A peak currents, along with the droplet size predicted from the static force balance theory. Steel electrodes shielded with Ar - 2% oxygen were used at base currents of 180 and 200 A. The load duty cycle was 5%. The pulsing parameters were selected such that there is no taper formation on the electrode. The droplet size was measured at the pulsing frequency,

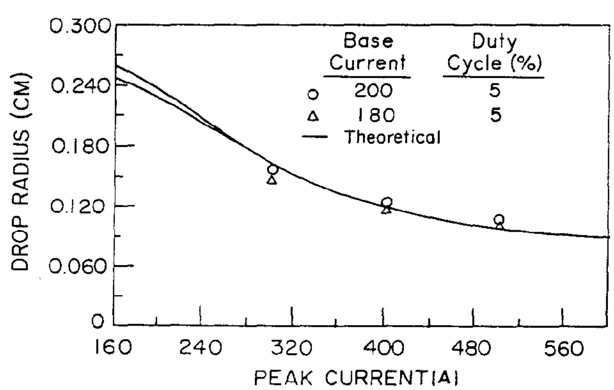

Fig. 18 — Comparison between the droplet size of the steel electrode form the static force balance theory and minimum droplet size from pulsed current welding. The shielding gas is Ar-2%O_2 Shielding.

which produces the minimum droplet sizes at a given peak current. As seen in the figure, the droplet size predicted from the static force balance theory agrees within ±10% with the experimental data. This experiment suggests that the cause of the deviation of droplet size in DC welding is tapering of the electrode tip.

Fig. 19 — Successive pictures of pendent drop motion prior to detachment from the steel electrode (total elapsed time: 60 ms). The shielding gas is Ar-2%O_2 shielding.

Comparison between the Static Force Balance Theory and the Pinch Instability Theory

The pinch instability theory and the static force balance theory have been used in modeling metal transfer with somewhat disappointing results. The drop size predicted from the pinch instability theory as in Equation 8 is unable to predict the trends of the measured drop size as seen in Fig. 6. One of the fundamental requirements for the pinch instability phenomena to occur is that the liquid metal should be in the form of cylinder, which is at a higher state of free energy than a corresponding liquid metal sphere. However, observation with a high-speed video camera shows that as soon as the solid metal melts, it forms a spherical liquid drop, which is already in the lower free energy state as compared with a cylindrical liquid column. Thus, there is no driving force, and it is not logical to apply the pinch instability theory to a problem in which a cylindrical liquid column never exists. Also, the repelled globular transfer mode and the effect of the electrode extension is very difficult to explain by the pinch instability theory. From these observations, it is concluded that the pinch instability theory is an inappropriate way to explain metal transfer phenomena in either globular transfer or projected spray transfer.

However, in streaming metal transfer mode, a liquid column instability phenomenon is observed as seen in Fig. 18. In this case, a cylindrical liquid jet is formed at the end of the electrode, and it disintegrates into several drops away from the electrode tip. As long as the diameter of the liquid jet remains the same, the droplet size will remain the same. This may explain the plateau of drop size in the high current range of streaming transfer as seen in Fig. 6. In this case, where a cylindrical liquid column exists the pinch instability theory might be applicable.

The modified static force balance theory predicts a larger drop size than the experimentally measured value in general. One of the possible causes of this deviation is the drop movement on the electrode as seen in Fig. 19. The figure shows successive pictures of pendant drop motion over a 60 ms period. Photographic analyses show that the peak velocity of the pendent drop reaches 20 cm/s and the dynamic force due to the pendent drop movement is calculated to be approximately 2 X 10^{-2} N. This is enough to account for the deviation of the drop size in the globular mode. Also, the surface tension value used in this study to calculate the holding force may be larger than the actual value of the system and, hence, may be incorrect. Combining these two effects, the predicted droplet size could be made to agree more closely with the experimentally measured data.

Conclusions

1) Metal transfer with steel electrodes shielded with Ar-2% oxygen shows a gradual transition, from globular to projected spray, followed by streaming transfer mode.

2) The static force balance theory can predict the droplet size in the globular transfer range, but it deviates significantly in the spray transfer range. The cause of the deviation is the geometry change of the electrode due to a taper formation at the electrode tip.

3) In order to analyze repelled globular transfer by the static force balance theory, it is necessary to determine another force that will act as a repelling force. A possible candidate for the repelling force is the cathode jet force on the drop.

4) When the taper is not formed, the static force balance theory can predict the droplet size very accurately in the spray transfer range, as has been shown in pulsed current welding.

5) The pinch instability theory fails to explain the effect of the electrode extension or of changes in the shielding gas on the metal transfer mode. The static force balance theory as modified by the taper formation can adequately explain metal transfer.

Acknowledgment

This research was funded by a grant from the United States Department of Energy under contract number DE-FG02-85ER-13331.

References

1. Lesnewich, A. 1958. Control of melting rate and metal transfer in gas-shielded metal arc welding: part - control of metal transfer. *Welding Journal* 37(9): 418-s to 425-s.
2. Smith, A. A. 1970. CO_2 welding of steel, The Welding Institute, Cambridge, U.K.
3. Amson, J. C. 1962. An analysis of the gas-shielded consumable metal arc welding system. British *Welding Journal* 41(4): 232–249.
4. Greene, W. J. 1960. An analysis of transfer in gas-shielded welding arcs. *Trans. AIEE* Part 2, 7: 194–203.
5. Waszink, J. H., and Graat, L. H. J. 1983. Experimental investigation of the forces acting on a drop of weld metal. *Welding Journal* 62(4):109-s to 116-s.
6. Lancaster, J. F. IIW Document No. 212-429-78.
7. Allum, C. J. 1985. Metal transfer in arc welding as a varicose instability: part 1—varicose instability in a current-carrying liquid cylinder with surface charge. *Journal of Physics D: Applied Physics* 18: 1431–1446.
8. Allum, C. J. 1985. Metal transfer in arc welding as a varicose instability: part 2—development of model for arc welding. *Journal of Physics D: Applied Physics* 18: 1447–1468.
9. Defize, L. F. 1962. Metal transfer in gas-shielded arcs. *Physics of the Welding Arc.* The Institute of Welding, London, U.K. 112–114.
10. Hezlett, T. B., and Gordon, G. M. 1957. Studies of welding arcs using various atmospheres and power supplies. *Welding Journal* 36(8): 382-s to 386-s.
11. Jahn, R. E. and Gourd, L. M. 1957. Gas-shielded welding of steel. British Commonwealth Welding Conference. The Institute of Welding, London, U.K., pp.148–155.
12. Elisstratov, A. P., Chernyshev, G. G., and Spitsyn, V. V. 1975. Transfer of electrode metal during welding in shielding mixtures. *Avt. Svarka* 12: 61–62.
13. Church, J. G. U.S. Patent #4463243, July 31, 1984.
14. Amson, J. C., and Salter, G. R. 1963. Analysis of the gas-shielded consumable metal-arc welding system-effect of ambient gas pressure. *British Welding Journal* 9: 472–483.
15. Perlman, M., Pense, A. W., and Stout, R. D. 1969. Ambient pressure effects on gas metal-arc welding of mild steel. *Welding Journal* (48)6: 231-s to 238-s.
16. Cameron, J. M ., and Baeslack, A. J. 1956. A straight-polarity, inert-gas process of welding mild steel. *Welding Journal* 35(5): 445–449.

17. Agusa, K., Nishiama, N., and Tsuboi, J. 1981. MIG welding with pure argon shielding-arc stabilization by rare earth additions to electrode wires. *Metal Construction* 9: 570–574.

18. Lucas, W., and Amin, M. 1975. Effect of wire composition in spray transfer mild steel MIG welding. *Metal Construction* 2: 77–83.

19. Needham, J.C., Cooksey, C. J., and Milner, D. R. 1960. Metal transfer in inert-gas shielded-arc welding. *British Welding Journal* 7(2): 101–114.

20. Waszink, J. H., and Van Den Heuvel, G. J. P. M. 1982. Heat generation and heat flow in the filler metal in GMA welding. *Welding Journal* 61: 269-s to 282-s.

21. Szekley, J. 1979. *Fluid Flow Phenomena in Metals Processing.* pp. 256–257. Academic Press, New York.

22. Waszink, J. H., and Graat, L. H. J. 1979. Der einflues der gasstroemung auf die tropfenabloesung beim plasma-mig scheissen. *Grosse Schweisstechnische Tagung,* DVS Berichte 57: 198–203.

23. Lord Rayleigh, 1897. *Proceedings of the Mathematical Society,* pp. 10, 4.

24. Lancaster, J. F. IIW Document No. 212-429-78.

25. Anno, J. N. 1977. *The Mechanics of Liquid Jets.* Lexington Books, Lexington, Mass.

26. Chapman, B. 1980. *Glow Discharge Processes.* John Wiley and Sons, New York, 53.

27. Mondain-Monval. The physical properties of fluids at elevated temperature. IIW Document No. 212-264–73.

28. *Hand Book of Chemistry and Physics,* 63rd ed. 1982. F-28, CRC Press, Boca Raton, Fla.

29. Eickhoff, S. T. 1988. Gas metal arc welding in pure argon. M.S. thesis, M.I.T., Cambridge, Mass.

30. Allemand, C. D., Schoeder, R., Ries, D. E., and Eagar, T. W. 1985. A method of filming metal transfer in welding arc. *Welding Journal* 64(1): 45–47.

31. Lin, M. L. 1985. Transport processes affecting the shape of arc welds. Ph.D thesis, M.I.T., Cambridge, Mass.

32. Kim, Y. S. 1989. Metal transfer in gas metal arc welding. Ph. D thesis, M.I.T., Cambridge, Mass.

33. Kim, Y. S., and Eagar, T. W. Metal transfer in pulsed current gas metal arc welding. To be published in *Welding Journal.*